

Three-dimensional crustal structure of Long Valley caldera, California, and evidence for the migration of CO₂ under Mammoth Mountain

G. R. Foulger,¹ B. R. Julian, A. M. Pitt, and D. P. Hill

Volcano Hazards Team, U.S. Geological Survey, Menlo Park, California, USA

P. E. Malin and E. Shalev

Division of Earth and Ocean Sciences, Nicholas School of the Environment, Duke University, Durham, North Carolina, USA

Received 2 November 2000; revised 15 March 2002; accepted 20 March 2002; published 12 March 2003.

[1] A temporary network of 69 three-component seismic stations captured a major seismic sequence in Long Valley caldera in 1997. We performed a tomographic inversion for crustal structure beneath a 28 km × 16 km area encompassing part of the resurgent dome, the south moat, and Mammoth Mountain. Resolution of crustal structure beneath the center of the study volume was good down to ~3 km below sea level (~5 km below the surface). Relatively high wave speeds are associated with the Bishop Tuff and lower wave speeds characterize debris in the surrounding moat. A low- V_p/V_s anomaly extending from near the surface to ~1 km below sea level beneath Mammoth Mountain may represent a CO₂ reservoir that is supplying CO₂-rich springs, venting at the surface, and killing trees. We investigated temporal variations in structure beneath Mammoth Mountain by differencing our results with tomographic images obtained using data from 1989/1990. Significant changes in both V_p and V_s were consistent with the migration of CO₂ into the upper 2 km or so beneath Mammoth Mountain and its depletion in peripheral volumes that correlate with surface venting areas. Repeat tomography is capable of detecting the migration of gas beneath active silicic volcanoes and may thus provide a useful volcano monitoring tool. **INDEX TERMS:** 7205 Seismology: Continental crust (1242); 7230 Seismology: Seismicity and seismotectonics; 8419 Volcanology: Eruption monitoring (7280); 8424 Volcanology: Hydrothermal systems (8135); 8124 Tectonophysics: Earth's interior—composition and state (old 8105); **KEYWORDS:** tomography, Long Valley, volcano, carbon dioxide, crustal structure, earthquakes

Citation: Foulger, G. R., B. R. Julian, A. M. Pitt, D. P. Hill, P. E. Malin, and E. Shalev, Three-dimensional crustal structure of Long Valley caldera, California, and evidence for the migration of CO₂ under Mammoth Mountain, *J. Geophys. Res.*, 108(B3), 2147, doi:10.1029/2000JB000041, 2003.

1. Introduction

[2] Long Valley caldera is a large silicic volcano in eastern California (Figure 1). It was formed by the cataclysmic eruption 760,000 years ago of 600 km³ of solid rock equivalent, which created a 32 km × 17 km ellipsoidal caldera that subsided 2–3 km [Bailey *et al.*, 1976; Hill *et al.*, 1985a; Bailey, 1989]. The majority of the erupted material formed the Bishop Tuff, which is up to ~1.5 km thick inside the caldera. Subsequently, a resurgent dome formed, which is now 10 km in diameter, 500 m higher than the surrounding moat. The moat lies at an average elevation of ~2100 m above sea level. Rhyolitic to basaltic volcanism later occurred in the caldera moat and on the resurgent

dome, and the moat became filled with flows interfingering with glacial till, lake sediments and landslide debris. A 2996-m-deep well drilled into the resurgent dome (Figure 1) encountered postcaldera rhyolite flows and domes in the upper 0.6 km, underlain by Bishop Tuff intruded with rhyolites to a depth of 1.8 km. Below this are metavolcanic and metasedimentary basement rocks that correlate with Sierra Nevada roof pendant rocks [McConnell *et al.*, 1995]. Magma is thought to be deeper than 3–4 km below sea level (bsl) beneath the resurgent dome [e.g., Hill *et al.*, 1985b]. The temperature at the bottom of the deep drill hole at 0.5 km bsl is only 100°C which suggests that magma is presently considerably deeper than this.

[3] The most recently active volcanic area is a north-south trending zone that includes Mammoth Mountain, a 3380-m-high, 200–500 ka dacite volcano on the southwest caldera rim, the 35–0.6 ka rhyolitic Inyo domes and Mono craters, and 250-year-old dacites in Mono Lake. The whole system is underlain by a dike-like feeder system [Eichelberger *et al.*, 1984; Fink, 1985; Miller, 1985]. Most of the

¹Also at Department of Geological Sciences, University of Durham, Science Laboratories, Durham, UK.

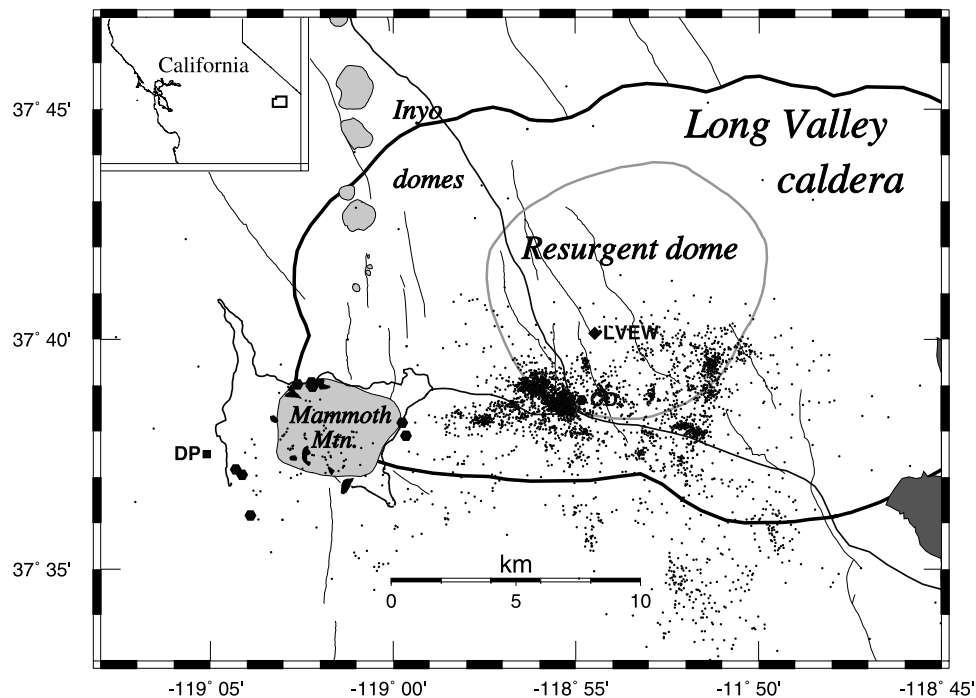


Figure 1. Map of central and western Long Valley caldera and vicinity. Mammoth Mountain and the Inyo domes are shown in light gray, and Crowley Lake is shown in dark gray. The Mono Craters and Mono Lake (not shown) form a 20-km northward continuation of the Mammoth Mountain/Inyo domes chain. Thick line is topographic margin of caldera; thin gray lines are faults; light gray line is resurgent dome; thin black lines are highways; black hexagons are CO₂-rich springs around Mammoth Mountain; black areas in and around Mammoth Mountain are sites where CO₂ degassing has killed trees [after *Farrar et al.*, 1995] (CD, Casa Diablo Hot Springs; LVEW, the 2996-m-deep Long Valley Exploration Well; DP, Devil's Postpile); and small dots are epicenters of 4873 earthquakes recorded on the 1997 temporary network, automatically picked and located using the final, three-dimensional crustal model COMB-20. Inset shows regional location of the main map.

present-day hot springs and fumaroles lie in an east trending zone along the southern edge of the resurgent dome and in the south moat, where geothermal fluid extraction is conducted at the Casa Diablo Hot Springs area. However, the south moat is not underlain by a primary heat upwelling; temperatures at Casa Diablo reach 175°C at 150–200 m below the surface but decrease with depth. The south moat thermal aquifers are thought to be recharged by lateral flow from a deep source in the west moat [*Sorey*, 1985].

[4] The present episode of seismic and volcanic unrest at Long Valley began in 1978 just south of the caldera and migrated into the caldera in 1980 [*Rundle and Hill*, 1988]. Much seismic activity has continued south of the caldera, particularly recently. Within the caldera, most earthquakes occur in the south moat, near Casa Diablo Hot Springs and along an inferred east-southeast trending, right-lateral, strike-slip, south moat fault [*Denlinger et al.*, 1985]. This fault has experienced ~3 m of slip since 1980. About 0.8 m of accumulated uplift of the resurgent dome has occurred during 1980–2000 (J. Langbein, personal communication, 2000) and requires the flow of ~0.3 km³ of magma into a region 4–8 km bsl beneath the dome. The deformation is not consistent with a single center of inflation, and separate centers at ~3 km bsl beneath the northern part of the dome and at ~11 km bsl beneath the southern part have been modeled [e.g., *Langbein*, 1989; *Langbein et al.*, 1995].

[5] An earthquake swarm of 6 months duration occurred beneath Mammoth Mountain in 1989 along with accelerated deformation and venting of volcanic gases [*Hill et al.*, 1990; *Sorey et al.*, 1993; *Hill*, 1996; *Cramer and McNutt*, 1997; *Sorey et al.*, 1998; *Wiemer et al.*, 1998]. In July, midway through the swarm, long-period (LP) earthquakes onset at depths of 7–20 km bsl southwest of Mammoth Mountain [*Pitt and Hill*, 1994]. Deformation data collected on geodimeter lines southeast of Mammoth Mountain are consistent with the opening of a ~13-cm-wide dike between –1 and 9 km bsl beneath Mammoth Mountain [*Hill et al.*, 1990; *Langbein et al.*, 1993].

[6] Increased heat flow, venting of CO₂ and temporal changes in ³He/⁴He ratios in a steam vent high on the mountain accompanied the 1989 activity. Sustained and widespread diffuse venting of CO₂ through the soil occurred subsequently killing large areas of trees around Mammoth Mountain. The total flux has been variously estimated at 200–300 t d⁻¹ [*Gerlach et al.*, 1999] and 500 t d⁻¹ [*Farrar et al.*, 1995]. This venting is now reduced by perhaps 20% in volumetric flow rate (M. Sorey, personal communication, 2000). *Sorey et al.* [1998] propose that the upper 2 km of Mammoth Mountain is relatively cold and dry and underlain by a 150°C, high-pressure gas pocket. This pocket might occupy some tens of cubic kilometers of porous and/or highly fractured rock, though smaller volumes also satisfy

the geochemical and flux modeling. The pocket is capped by an impermeable rock unit, such as a hydrothermally altered zone, and may lie above a CO₂-saturated liquid water reservoir. Slow leakage from the pocket may supply the long-lived CO₂-rich springs around Mammoth Mountain. The low-permeability cap ruptured in 1989, either by faulting or by a pressure increase, allowing gas to leak out at a much higher rate. The leakage is fault-controlled at shallow depth, with most of the surface areas of CO₂-induced tree kill lying on or close to known faults. The total amount of gas emitted during 1989–1997 is equivalent to the total degassing of <1.0 km³ of CO₂-saturated rock with a porosity of 0.01 [Sorey *et al.*, 1998] at pressures corresponding to the inferred depth of the pocket.

[7] A set of local earthquake data collected in 1989, supplemented by data collected on the Northern California Seismic Network (NCSN) 1989–1990, was used to obtain a tomographic image of the upper 4 km of Mammoth Mountain [Julian *et al.*, 1998]. That study provided compressional and shear wave (V_p and V_s) images that agree well with the known geological structure of the area. Directly beneath Mammoth Mountain a coherent, low- V_p/V_s body in the depth range –2 to 0 km bsl was detected, the outer boundary of which correlates with tree kill sites at the surface. Julian *et al.* [1998] suggest that the body imaged was a CO₂ reservoir that was either emplaced or ruptured in the earthquake swarm of 1989.

[8] Seismicity throughout much of the area was monitored in 1997 by the deployment of 69 seismic stations over a 300 km² area [Foulger *et al.*, 1998a, 1998b]. An intense swarm in the Casa Diablo Hot Springs-south moat area was recorded by our network. Frequent LP earthquakes occurred southwest of Mammoth Mountain, along with increased ³He/⁴He ratios in steam from fumaroles on Mammoth Mountain [McGee *et al.*, 2000]. The excellent earthquake data set collected enabled high-resolution tomography. The 1989 experiment and the Mammoth Mountain part of the 1997 experiment were very similar, and comparing the results enabled changes in structure in the interim 8-year period to be studied.

2. Data Collection

[9] Temporary seismometer networks were operated in the Long Valley area in June 1989 and May–September 1997. In both experiments, three-component 2-Hz Mark Products model L-22 sensors were used, and supplementary data were drawn from the NCSN network of vertical 1-Hz stations (Mark Products model L-4 sensors).

[10] The temporary network of June 1989 was deployed for 4 days on and around Mammoth Mountain in response to the onset of a vigorous swarm of earthquakes there (Figure 2). Twelve three-component stations were installed, recording in triggered mode on GEOS digital data loggers at 100 samples per second (sps) [Borcherdt *et al.*, 1985] (Table 1).

[11] The network deployed in 1997 covered a much larger area and recorded locatable earthquakes from 19 May to 30 September [Foulger *et al.*, 1998b]. The entire network comprised 63 three-component short-period sensors and six three-component broadband instruments (Figure 3 and Table 1). The western part of the network comprised 23

stations deployed on and around Mammoth Mountain by the U.S. Geological Survey and University of Durham, U.K. One objective of the experiment was to repeat the tomographic study of Mammoth Mountain that used the data collected in 1989 [Julian *et al.*, 1998]. Thus seven of the temporary sites occupied in 1989 were reoccupied in order to minimize errors caused by variable network geometry. Three stations were deployed at distances of up to 33 km to the north, south and west of Mammoth Mountain in order to improve focal sphere coverage of the deep, long-period (LP) earthquakes that occur beneath Devil's Postpile [Pitt and Hill, 1994]. These stations were maintained by foot in Wilderness areas not served by roads [Foulger *et al.*, 1998a]. Two stations had Guralp 3-CMG and 40-T broadband sensors.

[12] Data from the western part of the network were recorded on 16-bit REFTEK 72A-02 Data Acquisition Systems using GPS or OMEGA timing. The two broadband stations were recorded continuously on 24-bit REFTEK data loggers. Two data streams were recorded, the first continuously at 100 sps and the second as 10-s windows of data in response to a simple local earthquake trigger. Triggering times from the second stream were used a posteriori to identify time intervals of interest, for which data were extracted automatically from the continuous stream. The list of triggers contained the majority of locatable events recorded.

[13] The eastern part of the network was operated by Duke University. An additional objective of this part of the network was studying guided waves in the north-northwest trending fault zones that traverse the caldera. It comprised 36 stations recording in triggered mode at 500 sps on 24-bit REFTEK data loggers and four broadband stations recording continuous data [Stroujkova and Malin, 2000]. This part of the network covered densely the southern part of the resurgent dome and the south moat. The entire network covered uniformly an area of 300 km².

[14] The seismic rate in Long Valley in 1997 was low (<10 earthquakes per day) until the beginning of July. Shortly after all the temporary stations had been installed, a series of vigorous swarms occurred in the center of the network. The onset of activity commenced 3 weeks after a sharp increase in the rate of inflation of the resurgent dome was observed [Foulger *et al.*, 1998b]. Over 4000 locatable, high-frequency earthquakes were recorded 22 May to 30 September (Figure 1). The majority of the earthquakes occurred above 8 km bsl and clustered near Casa Diablo Hot Springs, but large numbers also occurred throughout our network and provided an excellent data set for the tomography. The south moat fault was intensely reactivated 22 November [Barton *et al.*, 1999], by which time we had decommissioned our network.

[15] The rate of occurrence of LP events beneath Devil's Postpile increased dramatically in early 1997, peaking at 19 events per week in April, and remained at an elevated level throughout our deployment period. We hand picked 20 LP events on the stations of the temporary network and these events, since they were located at depths greater than 8 km bsl beneath Devil's Postpile, greatly improved ray sampling beneath Mammoth Mountain. The picking errors for these events, from which S waves only could be measured, are about twice those of the S waves from the impulsive short-

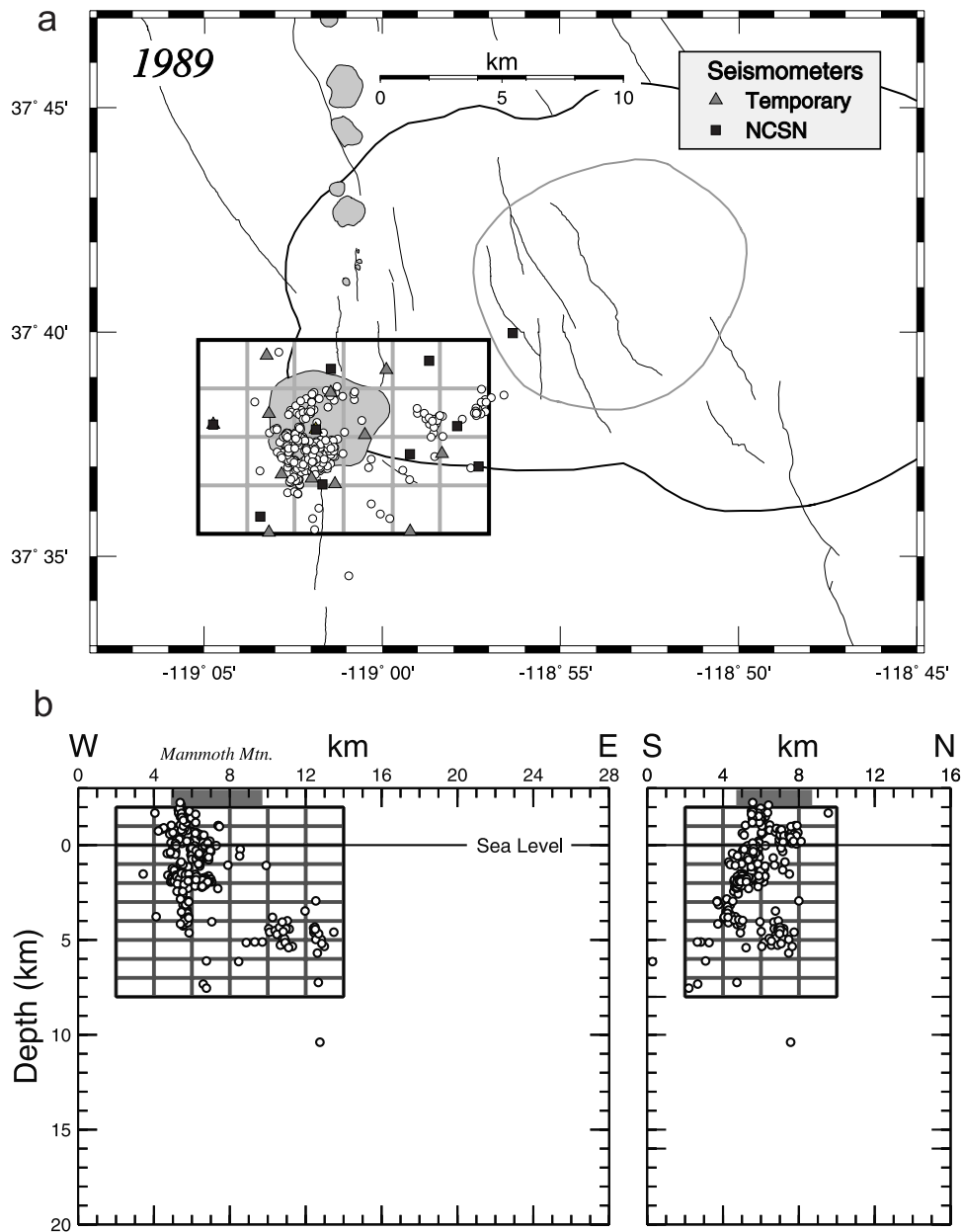


Figure 2. (a) Map showing the 1989/1990 seismic experiment. The tomography grid of *Julian et al.* [1998] is outlined in black, with grid lines shown in gray. Circles are epicenters of earthquakes used for tomography, relocated using model COMB-20. Other map features as for Figure 1. (b) (left) West-east and (right) south-north cross sections of the same region showing tomography grid and hypocenters of the earthquakes used in tomography, relocated using model COMB-20. Gray bars indicate position of Mammoth Mountain.

period earthquakes that composed the main body of the data set.

3. Data Processing and Tomographic Inversions

3.1. Data Processing and Inversion Technique

[16] The data recorded 1989–1990 and in 1997 were all processed in the same way. P and S wave arrival times were measured by hand from digital seismograms using the interactive seismogram processing program *epick* (B. R. Julian, unpublished computer program). The measured

Table 1. Details of the 1989/1990 and 1997 Experiments

	1989/1990	1997
Number of sensors		
Short-period three-component	12	63
NCSN vertical-only	10	17
NCSN three-component	–	2
Broadband three-component	–	6
Grid dimensions		
Area, km	12 × 8	28 × 16
Thickness, km	8	8
Number of nodes inverted for	421	2545

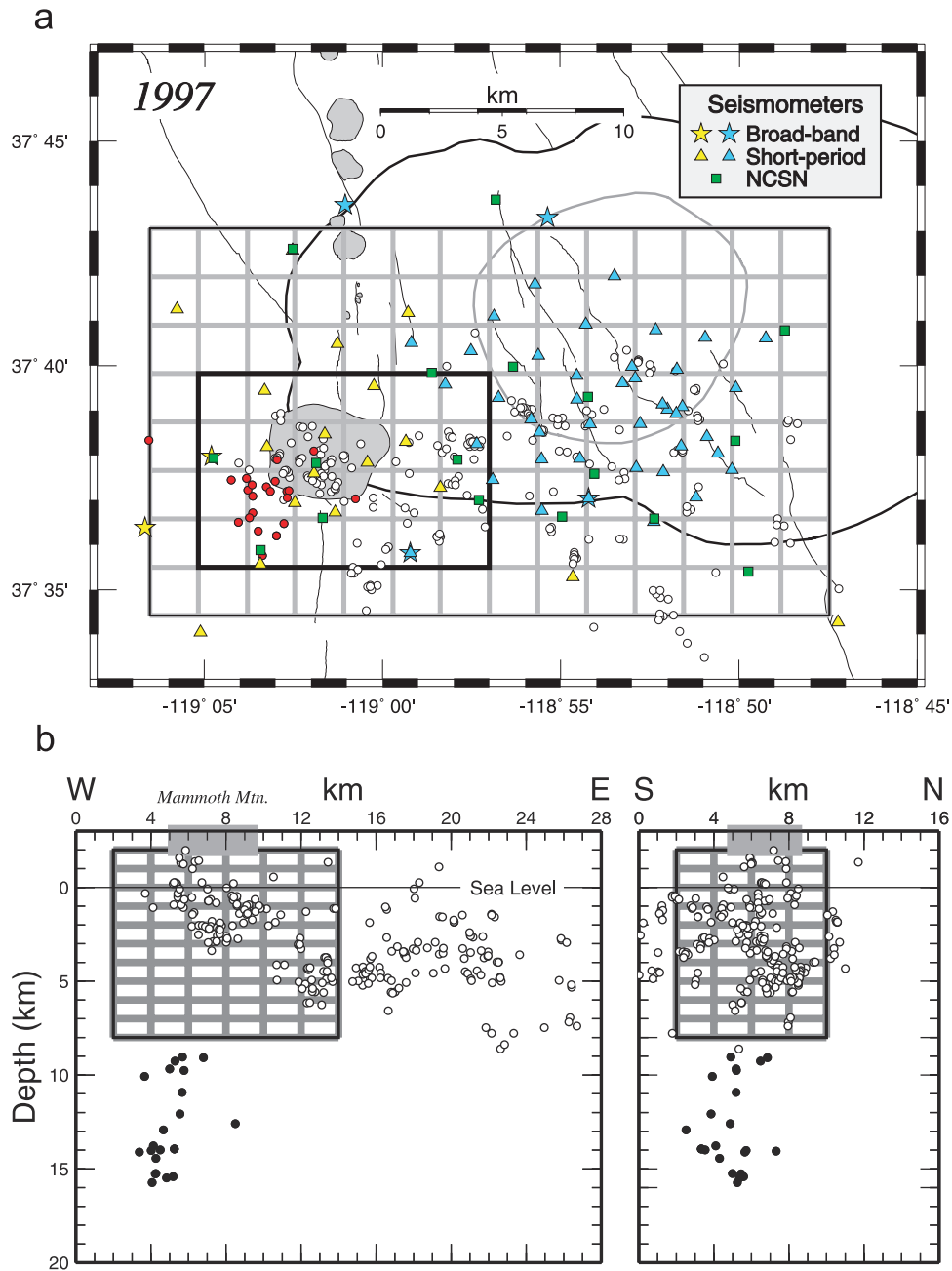


Figure 3. (a) Map showing the 1997 seismic experiment. Yellow triangles are stations of the western part of the network, which recorded continuously; blue triangles are stations of the eastern part of the network, which recorded in triggered mode. The broadband stations recorded continuously; circles are epicenters of earthquakes used for the tomography, relocated using model COMB-20; red dots are LP earthquakes. The tomography grid for models COMB-20 and COMB-5 is outlined in black, and the grid lines are shown in gray. The 12×8 km area imaged by *Julian et al.* [1998] using the 1989/1990 data, and used for models 1989-20 and 1997-20 in this paper, is outlined with heavy black line. (b) (left) West-east and (right) south-north cross sections showing hypocenters of the 1997 earthquakes used for the tomography, relocated using model COMB-20. Gray bars indicate position of Mammoth Mountain; black dots are LP earthquakes.

times are precise to ~ 0.01 s. Relatively few S wave arrival times were measured on NCSN stations, most of which lacked horizontal sensors. The number of observations used in the tomographic inversion, and inversion statistics, is shown in Table 2. In the case of the vast 1997 data set, for

which arrival time picking of each earthquake took more than an hour, events were carefully selected to yield as uniform a geographic distribution as possible (Figure 3). Where S wave birefringence was noted, the earlier S wave arrival was picked.

Table 2. Details of the Tomographic Inversions

Model	COMB-20	COMB-5	1989-20	1997-20
Data	1989/1990 + 1997	1989/90 + 1997	1989/1990	1997
Number of P phases	9983	9939	2701	7238
Number of S phases	4579	4567	1111	3456
Number of earthquakes	551	546	283	263
V_p damping, $s^2 \text{ km}^{-1}$	20	5	20	20
V_p/V_s damping, s	20	5	20	20
Variance reduction, %				
P	77	80	4	6
$S-P$	70	72	2	2
Final RMS residual, s				
P	0.048	0.045	0.043	0.045
$S-P$	0.110	0.106	0.080	0.115

[17] The data were inverted using the program SIMULPS12 [Thurber, 1983; Evans *et al.*, 1994]. This program uses an iterative, damped least squares method to invert arrival times, simultaneously estimating earthquake locations and three-dimensional V_p and V_p/V_s fields. The wave speeds are parameterized by values defined at the nodes of a three-dimensional grid, between which the V_p and V_p/V_s values are assumed to follow trilinear functions. The nodes were spaced at intervals of 2 km horizontally and 1 km vertically. The grid extended from -2 km bsl (i.e., 2 km above sea level) down to 5 km bsl. The floor of the caldera in the south moat is at about -2.2 km bsl. To continue values smoothly outside the three-dimensional grid, we included nodes on planes at distances of 50 km from the faces of the grid. The nodes are located so that a subset coincides with those used by Julian *et al.* [1998] in inverting the 1989/1990 data set. The starting one-dimensional wave speed model used was obtained from inverting the 1989/1990 data using the program velest [Kissling *et al.*, 1994; Julian *et al.*, 1998].

3.2. Combination of the 1989/1990 and 1997 Data

[18] In order to obtain an average wave speed structure for the Long Valley area, we combined the data from 1989/1990 and 1997. Our final model is constrained by 3868 arrival times from earthquakes recorded in 1989/1990 and 10,694 from earthquakes recorded in 1997, yielding a total of 14,562 arrival times (Table 2). A graded inversion approach was used. The nodes were initially spaced 4 km apart horizontally and two inversions were performed, first for V_p and then for both V_p and V_p/V_s simultaneously. The resulting structure was then interpolated to 2-km spacing and used as a starting model for a final pair of inversions. Damping trade-off curves, which show how model complexity varies with damping, were used at all stages to choose suitable damping values. We used values that gave a good balance between achieving a large data variance reduction and increasing model complexity [e.g., Foulger and Toomey, 1989; Julian *et al.*, 1996; Miller *et al.*, 1998] (Table 2). Our final model, COMB-20 (Figure 4) uses values of $20 \text{ s}^2 \text{ km}^{-1}$ for V_p and 20 s for V_p/V_s . Compared with studies that use values as low as $5 \text{ s}^2 \text{ km}^{-1}$ for V_p and 2 s for V_p/V_s [e.g., Foulger and Toomey, 1989; Foulger *et al.*, 1997], the values we used in this study are relatively high, and image only those structures that are strongly supported by the data. The inversion results were interpolated onto a 0.1-km grid using bilinear interpolation and

plotting using program grdimage [Wessel and Smith, 1998] (Figure 4).

3.3. Separate Inversions of the 1989/1990 and 1997 Data

[19] In order to investigate the possibility of changes in structure between 1989/1990 and 1997, we also inverted the 1989/1990 and 1997 data separately. Even in the absence of changes in the Earth, differences between imaged structures are expected, because of differences in source and sensor locations (and hence ray paths) and random observational errors [e.g., Arnott and Foulger, 1994; Gunasekera *et al.*, 2003]. We therefore adopted a conservative approach designed to minimize changes.

[20] A starting model was first obtained by inverting the combined data set using the low damping values of $5 \text{ s}^2 \text{ km}^{-1}$ for V_p and 5 s for V_p/V_s (model COMB-5). This absorbed as much signal as possible from the data into the structural model. This structure was then used to invert the 1989/1990 and 1997 data separately using the relatively high damping values of $20 \text{ s}^2 \text{ km}^{-1}$ for V_p and 20 s for V_p/V_s , which discouraged all but the most significant model changes (models 1989-20 and 1997-20). The results using the 1989/1990 and 1997 data, along with the differences, are shown in Figure 5, and inversion statistics are given in Table 2.

[21] A suite of damping values was tried and the results compared. Damping values of $5 \text{ s}^2 \text{ km}^{-1}$ for V_p and 5 s for V_p/V_s for the combined data set yielded the maximum data variance reduction possible. Starting structures obtained from inversions of the combined data set using higher damping values resulted in larger changes being imaged between 1989/1990 and 1997. For the separate inversions of the 1989/1990 and 1997 data, damping had to be increased to the extreme values of $80 \text{ s}^2 \text{ km}^{-1}$ for V_p and 80 s for V_p/V_s before essentially all changes were suppressed. The pattern of the changes was invariant with inversion strategy. We conclude that the absolute amplitudes of the changes detected and shown in Figure 5 are dependent on the damping values used in the inversions, but that the spatial pattern is real [Foulger *et al.*, 1995].

3.4. Location of Earthquakes Using the Final Three-Dimensional Model

[22] All the earthquakes from 1989/1990 and 1997 used for the tomography were relocated using model COMB-20, and their locations are shown in Figures 2 and 3. Only the small part of the 1997 data set used for the tomog-

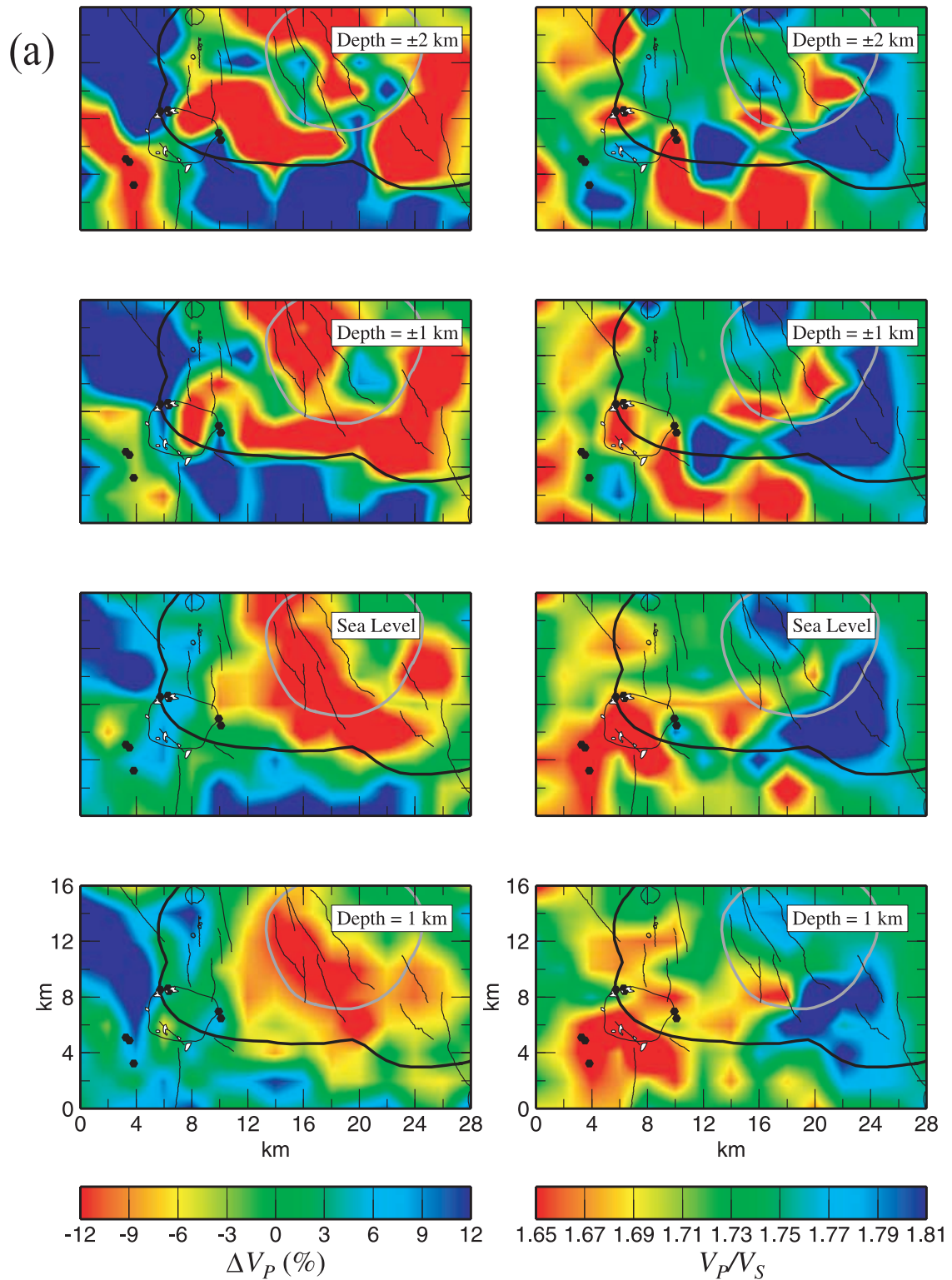


Figure 4. (a) (left) V_p and (right) V_p/V_s at four depths in the interval -2 to 1 km bsl, obtained from inverting the combined 1989/1990 and 1997 data (model COMB-20). Map features are as shown in Figure 1. Areas of tree kill around Mammoth Mountain are shown in white, and CO_2 -rich springs around Mammoth Mountain are shown as black hexagons. (b) Same as Figure 4a except for depths in the interval 2 – 5 km bsl.

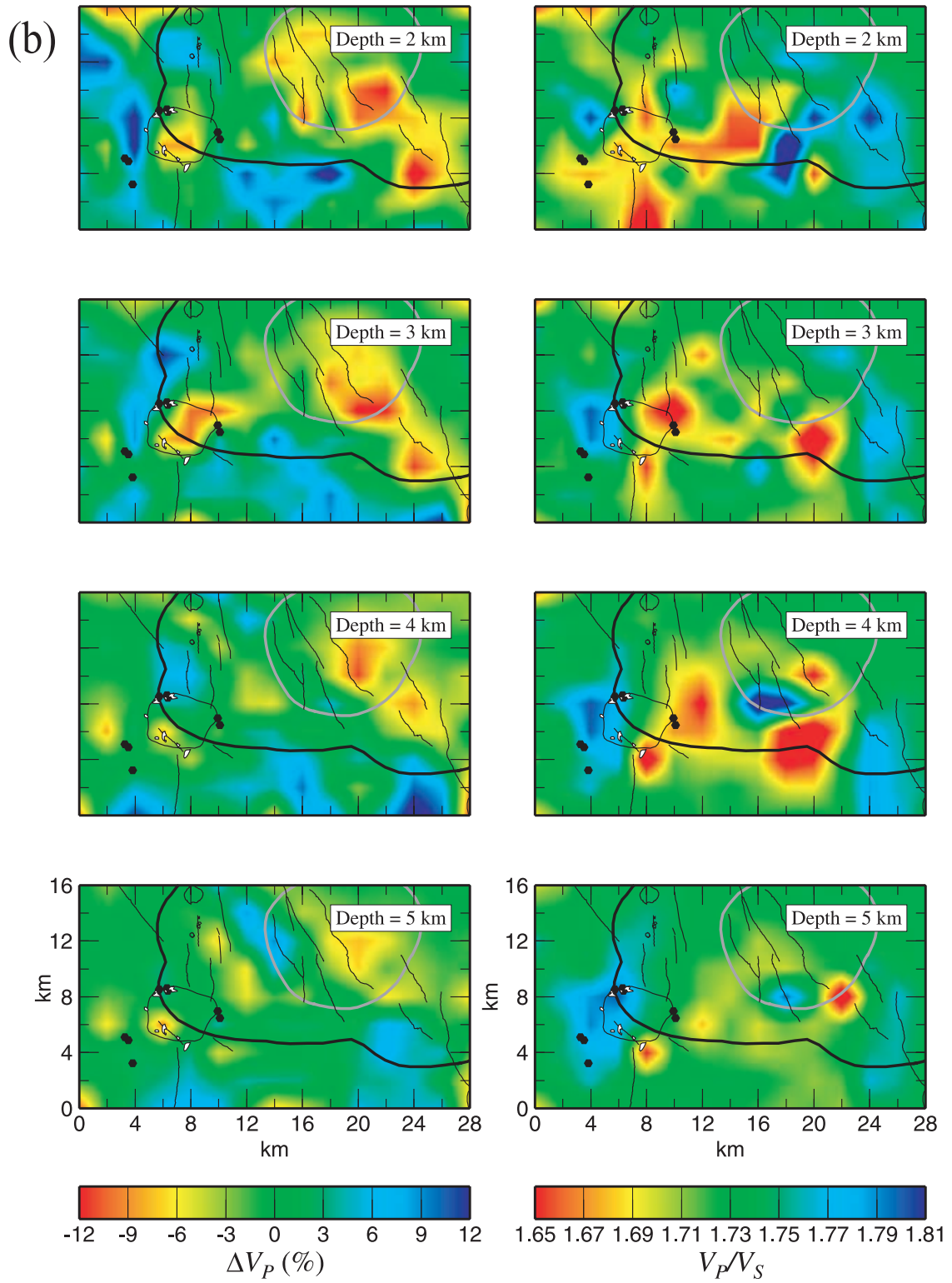


Figure 4. (continued)

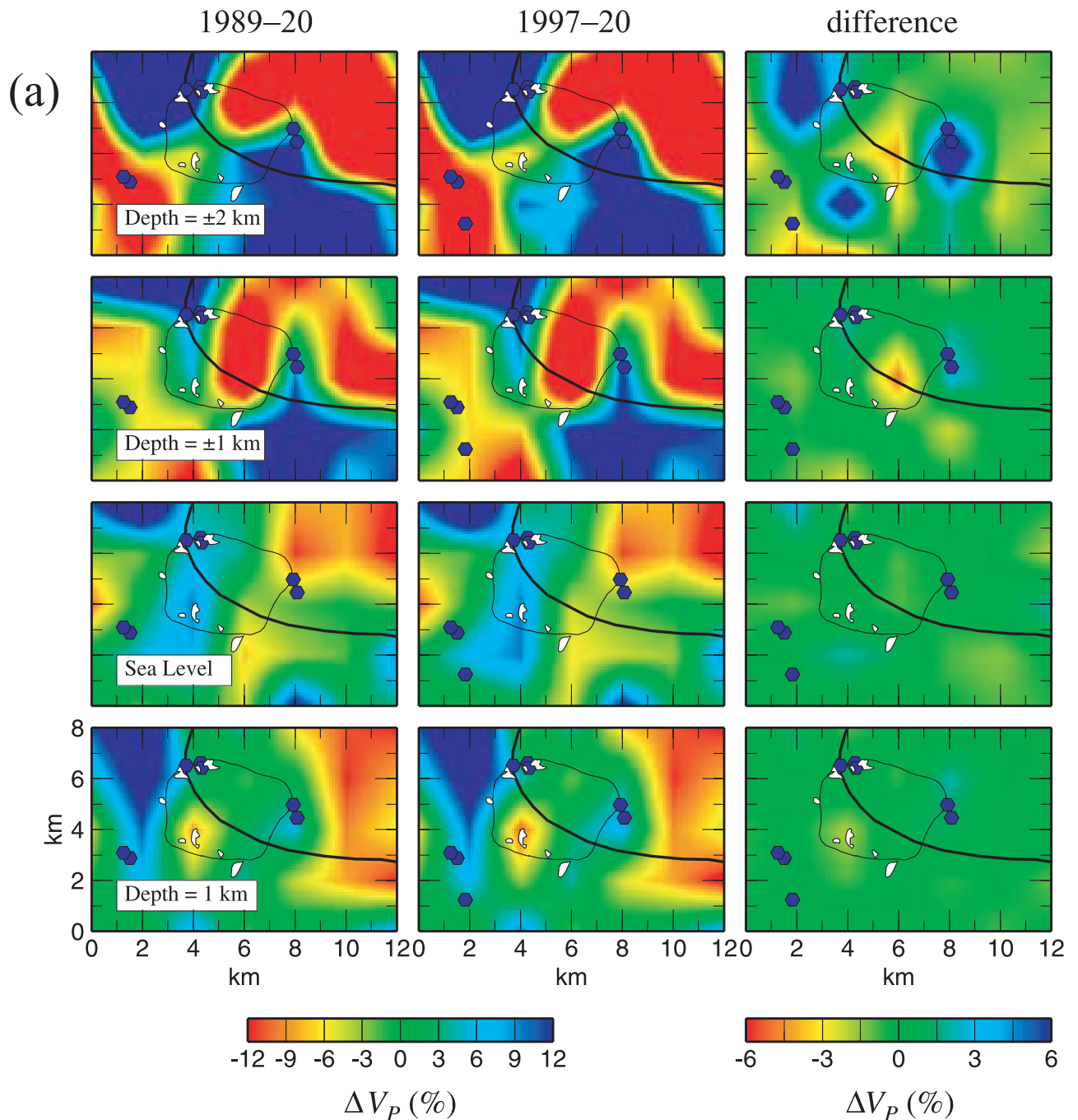


Figure 5. (a) V_p structure at four depths in the interval -2 to 1 km bsl for the Mammoth Mountain area (small box, Figure 3a). Map features are as shown in Figure 1. (left) Model 1989-20, showing structure obtained from inverting the 1989/1990 data using a model obtained from the combined data set (model COMB-5) as a starting model; (middle) model 1997-20, showing structure obtained from inverting the 1997 data using model COMB-5 as a starting model; (right) difference between the middle and the left panels. (b) Same as Figure 5a except for V_s . (c) Same as Figure 5a except for V_p/V_s .

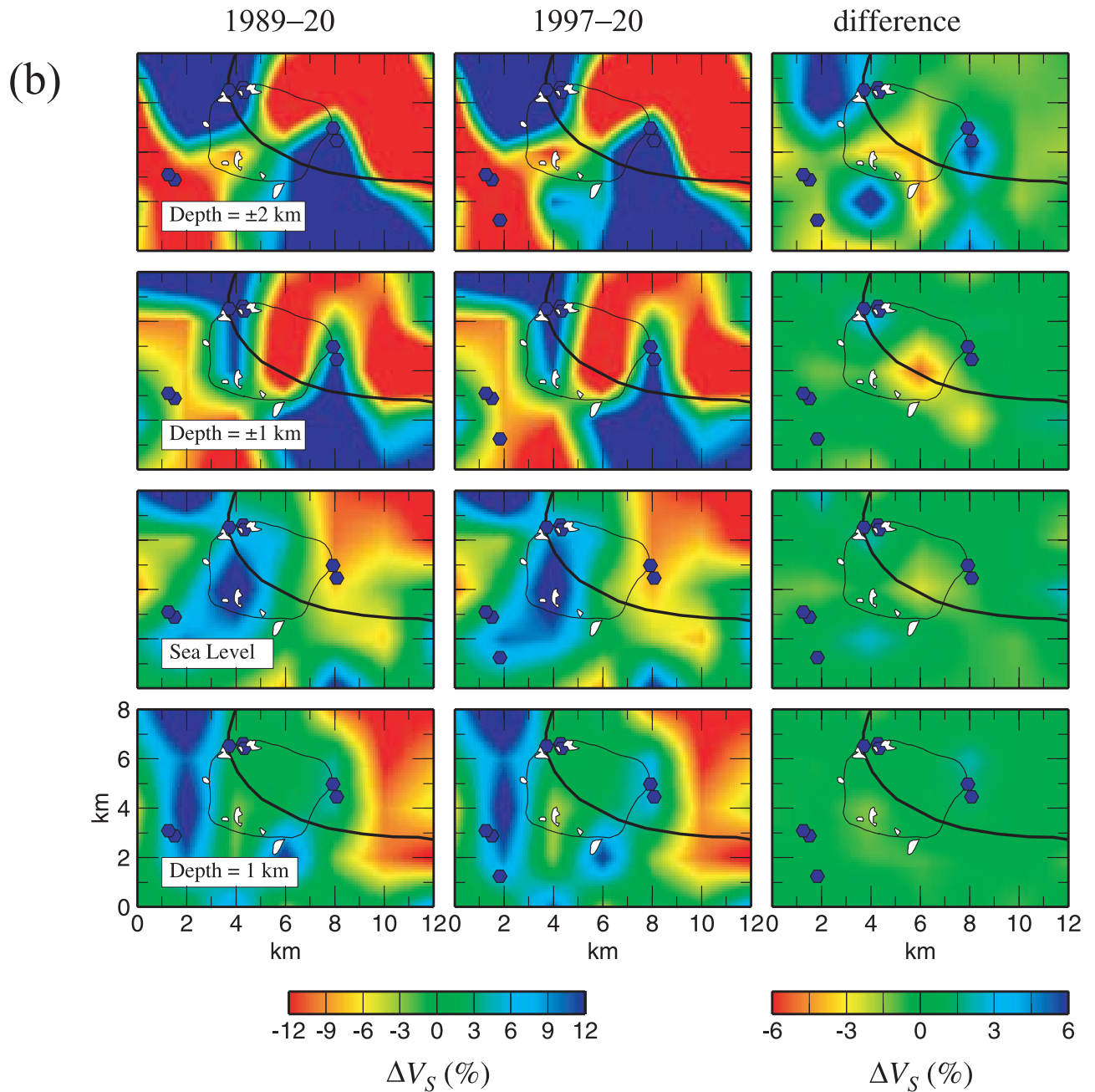


Figure 5. (continued)

raphy was picked by hand. The rest of the locatable earthquakes were picked automatically using an algorithm based on that of R. Crosson (personal communication, 1991). All those events were located by tracing rays through model COMB-20 using program qloc3d [Julian, 2000] and are shown in Figure 1.

4. Results and Discussion

4.1. Earthquake Distribution

[23] The 283 earthquakes recorded in 1989/1990 in the Mammoth Mountain area and used in the tomographic inversions mostly clustered beneath the southwest part of Mammoth Mountain (Figure 2). The hypocentral volume defined a north trending, vertical, blade-like structure

extending from near to the surface at its northern end to a depth of ~ 7 km bsl at its southern end (Figure 2b). Earthquakes were also distributed to the east and southeast of Mammoth Mountain. This distribution corresponds in general to that of the several thousand earthquakes located by NCSN for the whole 6-month swarm [Hill *et al.*, 1990]. Our locations are more spatially clustered and are probably more accurate because of the better crustal model and denser network used, but this also could be partly a consequence of our shorter monitoring period. Our best estimate for the orientation of the blade-like structure defined by our locations does not differ significantly from the strike of $N20^\circ E$ estimated by Hill *et al.* [1990].

[24] Most of the events recorded in 1997 formed an intense, northwesterly trending, bipartite cluster in the depth

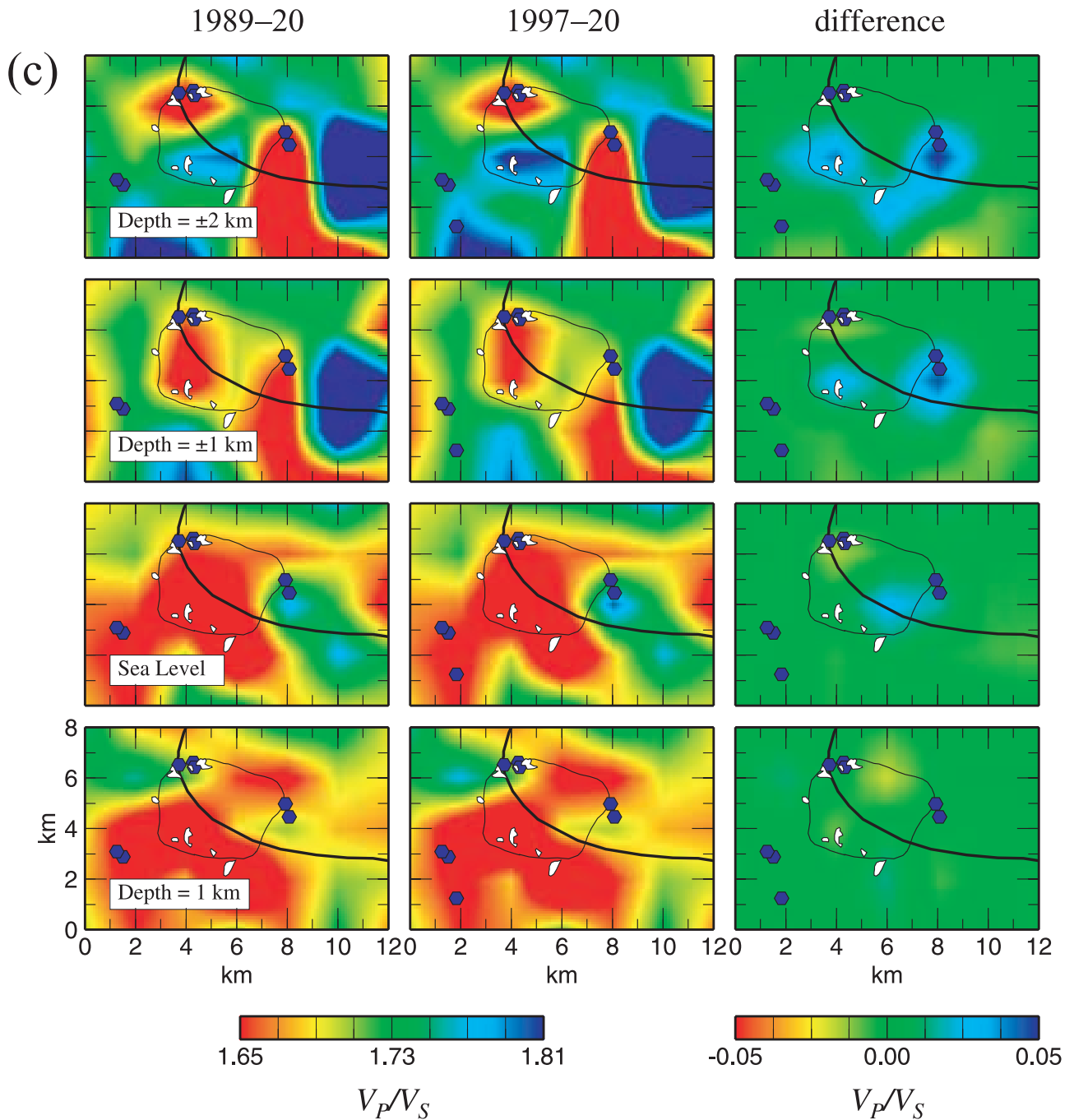


Figure 5. (continued)

range ~ 3 – 6 km bsl directly beneath Casa Diablo Hot Springs (Figures 1 and 3). Many earthquakes are clustered in a north-northeast trending zone beneath the southeastern part of the resurgent dome. In addition, diffuse activity and small clusters were scattered throughout the south moat, the southern part of the resurgent dome, and the Sierra Nevada south of the caldera. This distribution is similar to that which has characterized the region since the early 1980s. The maximum depth of high-frequency earthquakes in 1997 shallowed from ~ 8 km bsl beneath the eastern part of the south moat to 3 km bsl beneath Mammoth Mountain. If the base of the seismogenic zone at moderate

strain rates corresponds to the 250 – 300°C isotherm, as suggested by Hill [1992], then this suggests that such temperatures are reached at 3 km bsl beneath Mammoth Mountain (i.e., ~ 6 km below the summit). In 1989, earthquakes beneath Mammoth Mountain were observed up to ~ 8 km bsl (Figure 2), perhaps as a result of temporary high strain rates. The LP events measured in 1997 occupied a diffuse, 2-km-wide zone, in the depth range 8–16 km bsl southwest of Mammoth Mountain, which dips steeply to the west (Figure 3).

[25] The epicentral distribution of earthquakes in the Mammoth Mountain area during our monitoring period in

1997 was similar to that of 1989/1990. High-frequency earthquakes occurred shallower than 3 km bsl in both 1989/1990 and 1997, although no magma is thought to have been intruded in 1997. The intermediate depth range, 3–8 km bsl, that was seismically active in 1989 [Hill *et al.*, 1990] was aseismic during our 1997 monitoring period (Figure 3b). This volume may have been seismogenic in 1989 because of a high strain rate caused by deeper dike injection, or it may have hosted the upper part of the dike. The depth interval 4–6 km was also associated with earthquakes thought to be associated with fluid resonance [Cramer and McNutt, 1997], and a b value anomaly thought to indicate high pore pressure or temperature [Wiemer *et al.*, 1998]. The small dike thickness inferred from geodetic measurements (13 cm), and the 10-km height (–1.5 to 8.5 km bsl), implies an unusually large aspect ratio. The emitted gas was relatively cold, and contained no volcanic gases other than CO₂ [Sorey *et al.*, 1998], though this might be explained by groundwater scrubbing. These observations suggest that the deformation inferred to have occurred above ~3 km bsl may have been caused by the opening of a crack filled with high-pressure water or gas, rather than magma, and that magma injection may have been restricted to greater depths.

[26] The steep, westerly dipping zone of 1997 LP earthquakes between 8 and 16 km bsl projects to the surface at the eastern edge of Mammoth Mountain and appears to be a downward continuation of the shallower, 1989 seismogenic zone. The LP events are thought to indicate a zone where magma movement occurs at depth [Pitt and Hill, 1994]. It is thus also possible that magma intrusion in 1989 was limited to this zone only.

4.2. Structure Beneath Long Valley Caldera and Mammoth Mountain

[27] Both the V_p and the V_p/V_s fields in model COMB-20 show good agreement with the known geological structure of the area (Figure 4). Seismic wave speeds are as much as 1 km s⁻¹ low inside the caldera above sea level, and the correlation of V_p with the caldera boundary and the edge of the resurgent dome is very good. In the upper 2 km, the V_p/V_s field is dominated by low anomalies beneath the western and southwestern part of the caldera rim. The low- V_p , high- V_p/V_s anomalies in the moat of the caldera in the upper 2 km correlate with the low-density postcaldera rhyolitic flows, interfingered glacial till, landslide debris and lake sediments. These anomalies are bounded sharply by the resurgent dome, which is characterized by higher wave speeds because of updoming of the Bishop Tuff as demonstrated by geologic mapping [Bailey, 1989] and deep drilling [McConnell *et al.*, 1995]. Rocks similar to those in the moat also appear to comprise that part of Mammoth Mountain inside the caldera and above sea level. Some zones of higher wave speed imaged at shallow depth in the moat west of the resurgent dome, beneath the Inyo domes area, and directly south of the resurgent dome suggest that the moat fill is discontinuous or heterogeneous.

[28] High- V_p and low- V_p/V_s values characterize the Sierran crystalline rocks outside the caldera, except in the vicinity of Mammoth Mountain. The high- V_p , low- V_p/V_s block within the caldera immediately east of Mammoth

Mountain above sea level may be a slump of Sierran rocks into the caldera (R. Bailey, personal communication, 1999). In the depth range –1 to 1 km bsl, V_p is as much as 17% lower in the western half of the resurgent dome than in the eastern half. The base of the Bishop Tuff in the dome is known from drilling to lie at about –0.7 km bsl (Figure 1) and to be underlain by competent basement rocks. The western half of the resurgent dome is dissected by several major faults and is probably more tectonically active, richer in pore fluids and hotter than the eastern part. It is also associated with anomalously high b values, which are thought to correspond to high pore pressure, temperature and fracture density, or low stress [Wiemer *et al.*, 1998]. These independent studies are thus in agreement, and supported by an easterly deepening of the base of the seismogenic layer beneath the resurgent dome from ~5 to 8 km [Hill, 1992].

[29] Low wave speeds are restricted to the southern part of the resurgent dome at depths of 2–3 km bsl. The depth to the base of the seismogenic layer is at ~4 km bsl beneath this area, and an inflation center is modeled at a depth of 4 km bsl on the basis of surface deformation data [Langbein, 1989]. These results suggest that the 500°C isotherm may lie at ~4 km depth in this area. Magma may be ruled out as an explanation for the low- V_p anomalies beneath the western and southern portions of the resurgent dome at 0–3 km bsl since this would be expected to be characterized by high V_p/V_s anomalies, which are not observed, as well as elevated temperatures at 3 km depth.

[30] Inversion of the 1989/1990 data provided the first detailed image of the volume beneath and around Mammoth Mountain [Julian *et al.*, 1998]. A coherent low- V_p/V_s anomaly of up to 9%, was imaged from ~11 to 1 km bsl beneath Mammoth Mountain. The edge of this anomaly correlated closely with areas of surface CO₂ venting, which led Julian *et al.* [1998] to interpret it as a leaky CO₂ reservoir. This anomaly is also imaged in both models COMB-20 and 1997-20, where it is continuous from –1 km to 2–3 km bsl. The addition of the 1997 data to the 1989/1990 data allowed a greater volume to be studied, showing the anomaly to be larger than imaged using the 1989/1990 data alone [Julian *et al.*, 1998]. The portion above sea level appears to be part of a chain of such anomalies that lie mostly outside but adjacent to the western and southwestern parts of the caldera (Figure 4). These anomalies thus occupy Sierran rocks rather than moat rhyolites or Bishop Tuff.

[31] A subsidiary low- V_p/V_s anomaly lies adjacent to the Casa Diablo Hot Springs geothermal area and extends from near the surface to 2 km bsl. This is most readily explained by increased vapor content in pores and fractures throughout a localized zone approximately 2 km² in area and extending from the surface to ~2 km bsl. High temperatures would be expected to lower V_s more than V_p , thus raising V_p/V_s . This suggests that the volume beneath Casa Diablo Hot Springs is probably not anomalously hot compared with its surroundings. These findings are in agreement with our understanding of the Casa Diablo Hot Springs geothermal area from drilling and geothermal prospecting. The area does not represent a primary zone of upwelling within which temperature would be expected to increase with depth. The present findings suggest, however, that a highly

fractured, potential geothermal fluid containment volume may extend to 2 km bsl. In contrast, studies of the attenuation of seismic waves have been interpreted to indicate a cupola-shaped intrusion of magma extending up to ~ 2 km bsl beneath Casa Diablo Hot Springs [Sanders and Ryall, 1983; Sanders, 1984]. Such a body would be expected to exhibit low V_p and high V_p/V_s , for which we find no evidence. Our results are in agreement with the observation that no thermal anomaly overlies the proposed cupola [Sorey, 1985].

[32] V_p/V_s anomalies may be caused by a variety of effects, and interpretation is ambiguous in the absence of independent constraints. Low- V_p/V_s anomalies may be caused by either low V_p or high V_s , both of which could be related to lithology. In addition, V_p is lowered by increased percentage of pore volume occupied by gas. V_s may be raised by decreasing pore pressure and stiffening the rock, e.g., by drying, as has been reported from The Geysers geothermal area [Boitnott, 1995; Boitnott and Boyd, 1996]. The chain of low- V_p/V_s anomalies south and west of Mammoth Mountain may thus be due to different factors, and apparently continuous anomalous zones may not all be related to a single effect. The low- V_p/V_s anomaly beneath Mammoth Mountain is shown by the 1997 data to broaden with depth below sea level and to extend to at least 1 km bsl.

4.3. Comparison With Previous Tomographic Models

[33] No V_p , or V_p/V_s , tomographic study of the Long Valley area using a station density comparable to that of this study has hitherto been reported. Two regional-scale studies of the area have been conducted, mostly using local and regional earthquakes recorded on the permanent regional networks [Kissling, 1988; Tryggvason, 1998]. Kissling [1988] studied an area 350×400 km in size, centered on Long Valley caldera, and parametrized by blocks with uniform wave speed ranging in horizontal dimension from 2.5 to 10 km and in thickness in the upper 15 km from 1.5 to 4 km. The data set comprised $\sim 80,000$ P wave arrival times for 3800 earthquakes at epicentral distances of up to 150 km, recorded at 200 stations. The model was calculated when local and regional earthquake tomography was in its infancy, but some features common with our model are discernible. Above sea level, high wave speeds were detected in the Sierran rocks to the south and west of the caldera and beneath the resurgent dome, with lower wave speeds in the caldera moat and the Mammoth Mountain area. Between -0.5 and 1 km bsl the high wave speeds beneath the resurgent dome were found to give way to low wave speeds, in agreement with our model.

[34] Tryggvason [1998] used the method of Benz *et al.* [1996] to study a 128×128 km region encompassing the caldera and surroundings. 80 stations of the NCSN and University of Nevada, Reno, networks were used, supplemented by data from temporary stations and seismic refraction lines. For their P wave model, Tryggvason [1998] used 3614 earthquakes and 20 explosions, which yielded 77,000 arrival times, and for their S wave model, 6110 earthquakes that yielded 15,500 arrival times. The inversion grid was parametrized on a scale of 2×2 km for P and 4×4 km for S in the horizontal, and 1 km in the vertical.

[35] Tryggvason [1998] show horizontal sections for the depth intervals -1 to 0 km bsl and $2-3$ km bsl that may be compared with our results. The agreement between the two P wave models is good. In the depth range -1 to 0 km bsl, both models image high P wave speed in the Sierran rocks outside the caldera to the west and south, and lower wave speeds beneath Mammoth Mountain and within the caldera. The higher wave speeds that we find associated with the resurgent dome, and the very low wave speeds associated with the moat fill, are not detected by Tryggvason [1998], however. A significant low P wave speed body detected by Tryggvason [1998] within the caldera east of the resurgent dome could not be confirmed by our study since it is peripheral to our network. At $2-3$ km bsl, both models detect relatively low P wave speeds beneath the resurgent dome and associated with Mammoth Mountain, along with high wave speeds outside the caldera.

[36] The V_p/V_s anomalies we determine are sufficiently small that our S wave model is visually similar to our P wave model. The P and S wave speed models of Tryggvason [1998] differ substantially, however, and thus the agreement with our S wave speed model is poorer. High wave speeds associated with the Sierran rocks south of the caldera are common to both S wave models. The S wave speed model of Tryggvason [1998] does not extend west of the caldera, so the high wave speeds that we detect there cannot be confirmed. The high wave speeds that we observe beneath the resurgent dome between -1 and 0 km bsl are not observed by Tryggvason [1998], nor are low S wave speeds beneath the resurgent dome and Mammoth Mountain at 2 km bsl. The poorer correspondence of the two models in the case of the S wave speed models may be a result of the coarser parameterization used by Tryggvason [1998].

4.4. Changes in Structure From 1989/1990 to 1997

[37] The structures imaged in the Mammoth Mountain area by independent inversions of the 1989/1990 and 1997 data sets (models 1989-20 and 1997-20) are similar in all first-order respects (Figure 5). Significant second-order differences are, however, detected beneath Mammoth Mountain, and to the northwest, southwest, south, and east (Figure 5, right panels). Directly beneath and to the south of Mammoth Mountain, a reduction in both V_p and V_s is detected in a north-south elongated zone that lies 2 km east of the zone that was seismogenic in 1989. V_s decreased by up to 6% between 1989/1990 and 1997, whereas V_p decreased by only up to 3%. To the northwest, southwest and east of Mammoth Mountain are volumes where both V_p and V_s increased. To the southwest, both V_p and V_s increased by up to 6%. To the east of Mammoth Mountain, V_p increased by up to 9%, whereas V_s increased by only up to 5%.

[38] The change in the V_p/V_s field is a coherent increase throughout a zone that encircles the southern half of Mammoth Mountain. Three maxima occur within this zone, beneath the southwestern part of Mammoth Mountain, to the south and to the east. The largest increase, of 3%, occurs in the eastern maximum. The whole zone correlates with surface areas experiencing significant CO_2 degassing (Figure 5c). The areas of V_p/V_s increase beneath southwest Mammoth Mountain and to the south directly underlie the Reds Creek and Horseshoe Lake tree kill areas have been

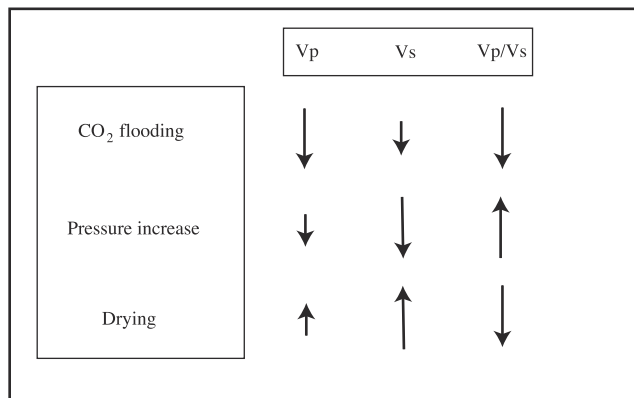


Figure 6. Schematic figure illustrating the effects of relevant processes on V_p , V_s , and V_p/V_s . Large arrows indicate the dominant effect, and small arrows indicate subsidiary or negligible effects.

estimated to vent over four times as much as all the other tree kill areas combined [Sorey *et al.*, 1998]. The strong maximum east of Mammoth Mountain is not associated with surface tree kill, but is overlain by the cold CO₂-rich Valentine soda spring and Chair 15 spring. The possibility that the changes we observe in V_p , V_s , and V_p/V_s result from migration of pore fluids beneath Mammoth Mountain thus warrants consideration.

[39] Theoretical relations linking changes in V_p , V_s , and their ratio with changes in pore fluid compressibility [Krief *et al.*, 1990; Mavko *et al.*, 1995; Mavko and Mukerji, 1995], and laboratory experiments measuring seismic wave speeds in sandstones saturated with hydrocarbon and CO₂ [Wang and Nur, 1989] show that V_p decreases significantly with CO₂ flooding because of an increase in bulk compressibility (Figure 6). V_s is affected little by flooding, resulting in a decrease in the V_p/V_s ratio. The magnitude of the effect is dependent on confining and pore pressure, temperature, porosity and permeability. However, in a recent study in the McElroy oil field, Texas, the effect of flooding of the oil reservoir in situ with CO₂ showed that the pore pressure increase accompanying CO₂ flooding reduced V_s by approximately the same percentage as V_p was reduced by the increase in compressibility of the bulk rock [Wang *et al.*, 1998]. This shows that in the case of bulk rock in situ, flooding with CO₂ may leave the V_p/V_s ratio unchanged. A decrease in V_p/V_s would be expected with CO₂ flooding accompanied by little pressure increase, and an increase in V_p/V_s would accompany CO₂ depletion with little pressure decrease.

[40] The McElroy oil field is a reasonable analog of the shallow levels beneath Mammoth Mountain. The CO₂ flooding occurred at a depth of 900 m below surface, where the reservoir rock is composed of dolostones and evaporite cement. Porosity and permeability are variable, with an average porosity of 10% and permeabilities in the range $0.01-90 \times 10^{-11} \text{ cm}^2$. Porosities and permeabilities of the shallowest 2–3 km beneath Mammoth Mountain are unknown. At the time of CO₂ flooding, the pore fluid in the McElroy field was half water and half oil with a density of 0.85 g cm^{-3} at 16°C and 1 atm pressure. The wave speed changes observed were considerably greater than predicted

using the Gassmann equation [Gassmann, 1951], which does not take into account changes in lattice properties caused by pressure, and were as high as -10% [Wang *et al.*, 1998]. This made it feasible to monitor the CO₂ flooding of the reservoir seismically.

[41] Influx of CO₂ beneath Mammoth Mountain is expected to be associated with a pressure increase, and CO₂ depletion is expected to be associated with pressure decrease. This association of changes in pore fluid phase and pressure would tend to make the effect of changes in V_p and V_s on the V_p/V_s ratio cancel out. A clearer picture of the pattern of CO₂ migration is thus more likely to be revealed by changes in V_p and V_s separately. The western and southern parts of the zone of increased V_p/V_s in the Mammoth Mountain area result from decreases in V_p along with larger decreases in V_s (Figures 5a and 5b). Such changes could be explained by influx of CO₂ accompanied by a relatively large increase in pore pressure. The eastern part of the increased V_p/V_s zone results from increase in V_p relative to V_s there and is consistent with depletion of CO₂ accompanied by a minor decrease in pore pressure. Approximately equal reductions in both V_p and V_s occur beneath the center of Mammoth Mountain, resulting in no change in V_p/V_s , which could be explained by an influx of CO₂ accompanied by an intermediate pressure increase. To the northwest and southwest approximately equal increases in both V_p and V_s occur, which are consistent with CO₂ depletion accompanied by an intermediate pressure decrease. These results suggest that changes in V_p and V_s separately may provide a clearer picture of the migration of CO₂ beneath Mammoth Mountain than changes in V_p/V_s .

[42] The present results suggest that in the period between 1989/1990 and 1997, gas migrated into a volume in the top 2.5 km beneath the center of Mammoth Mountain approximately overlying the dike or crack that opened in 1989. The source of this CO₂ may be the gas reservoir thought to underlie Mammoth Mountain below ~ 2 km below surface [Sorey *et al.*, 1998], or the flanking porous volumes to the southwest and east that are apparently leaking. Depleting the source volumes to the northwest and southwest of Mammoth Mountain may supply gas to the areas of tree kill adjacent to them. No significant changes in V_p and V_s were imaged at depths greater than ~ 2.5 km below surface. However, this may be because the compressibility of gas decreases with increasing depth and overburden pressure, rendering seismic wave speeds progressively less sensitive to changes in gas content with depth.

[43] The study of CO₂ flooding of the McElroy oil field, and our observation of variations in V_p and V_s between 1989/1990 and 1997 suggest that there is a direct correspondence between V_p/V_s anomalies and CO₂ saturation at a given depth only in the absence of significant lateral variations in lithology, temperature, porosity and pressure. Changes in V_p and V_s between 1989/1990 and 1997 suggest spatial changes in both gas saturation and pressure that imply that the CO₂ reservoir is more extensive than the low- V_p/V_s anomaly. At -2 km bsl, reduction in V_p and V_s is observed beneath the center and south of Mammoth Mountain and increase is observed to the southwest. The V_p/V_s anomaly is discontinuous in these regions, but the changes suggest that the CO₂ reservoir extends there also.

[44] These results contribute to a very small body of observations of temporal changes in V_p , V_s , and V_p/V_s accompanying the migration of pore fluids. A similar study performed in The Geysers geothermal field, California, detected a reduction of up to 0.07 or 4% in V_p/V_s 1991–1994 in volumes that were depleted of geothermal fluids by commercial exploitation. At The Geysers, the extraction of steam reduces pressure and causes pore water to flash to steam, and thus changes in both the fluid phase and the pore pressure reinforce each other to reduce V_p/V_s [Foulger et al., 1997; Gunasekera et al., 2003]. This situation contrasts with that at Mammoth Mountain where flooding with CO₂ is expected to correlate with pore pressure increase, causing the two effects to partially cancel out. A third factor reinforces the V_p/V_s decrease at The Geysers. The Franciscan graywacke sandstones that comprise the main reservoir rock are unusual in that the shear modulus increases with drying [Boitnott, 1995], which increases V_s , an effect not expected at Mammoth Mountain (Figure 6).

[45] Detectable reductions in V_p/V_s are expected to characterize zones of depletion in exploited geothermal areas. In the case of active volcanoes, however, changes in the V_p/V_s field may be a less reliable indicator of patterns of fluid migration because the effects of changes in fluid phase and pore pressure are expected to partially cancel out. In the case of active volcanoes, changes in the V_p and V_s fields must therefore be considered separately. The results nevertheless suggest that repeat tomography has the potential to provide a valuable tool for monitoring gas migration in volcano edifices.

5. Conclusions

[46] We make the following conclusions:

[47] 1. The crack that opened beneath Mammoth Mountain in 1989 may have been intruded with magma only below 3 or 8 km bsl, and shallower levels may have been filled by gas and/or water.

[48] 2. The postcaldera rhyolitic flows, interfingered lava flows, glacial till, and landslide debris that fill the south moat are associated with low wave speeds and relatively high V_p/V_s , and are up to ~2 km thick.

[49] 3. The Bishop Tuff beneath the resurgent dome is associated with relatively high V_p and V_s and average V_p/V_s . Low wave speed material is present at all depth intervals, however, particularly beneath the western half of the dome, and may indicate more fractured, porous, hotter material.

[50] 4. Sierran rocks outside the caldera to the south and the west are associated with high V_p and V_s .

[51] 5. The CO₂ reservoir that supplies surface venting extends from the surface to at least 1 km bsl, a thickness of 3.2 km.

[52] 6. V_p/V_s anomalies north of Mammoth Mountain, outside the western perimeter of the caldera, may indicate additional CO₂-saturated porous volumes or lithological variations.

[53] 7. A zone of increased vapor content in pores and fractures may extend from the surface to ~2 km bsl near Casa Diablo Hot Springs.

[54] 8. In the upper 2 km, between 1989/1990 and 1997, CO₂ may have flowed into the center of Mammoth Mountain

and become depleted in flanking volumes to the northwest, southwest and east.

[55] 9. Repeat tomography may provide a valuable tool for monitoring gas migration in volcano edifices.

[56] **Acknowledgments.** We thank the Natural Environment Research Council (NERC) and IRIS-PASSCAL for loans of instruments (NERC loan 540/0197), the U.S. Forest Service for permission to deploy seismic stations and assistance, and Dan Lister of the Mono County Government for practical assistance. The California Institute of Technology contributed two broadband seismometers with 24-bit data loggers and auxiliary equipment to the fieldwork. A. Strujkova, D. Schleupner, P. Boyd, R. Perthro, L. E. Foulger, N. Dotson, G. Sharer, E. Brodsky, M. Alvarez, and A. Newman contributed to the fieldwork. We thank Paul Davis of UCLA for lending a 24-bit REFTEK data logger during the 1997 field experiment. The manuscript was improved by valuable reviews by W. C. Evans, R. A. Bailey, J. C. Eichelberger, and S. R. McNutt.

References

- Arnott, S. K., and G. R. Foulger, The Krafla spreading segment, Iceland, 1, Three-dimensional crustal structure and the spatial and temporal distribution of local earthquakes, *J. Geophys. Res.*, *99*, 23,801–23,825, 1994.
- Bailey, R., Geologic map of Long Valley caldera, Mono-Inyo Craters volcanic chain, and vicinity, eastern California, map, U.S. Geol. Surv., Menlo Park, Calif., 1989.
- Bailey, R. A., G. D. Dalrymple, and M. A. Lanphere, Volcanism, structure, and geochronology of Long Valley caldera, Mono County, California, *J. Geophys. Res.*, *81*, 725–744, 1976.
- Barton, D. J., G. R. Foulger, J. R. Henderson, and B. R. Julian, Frequency-magnitude statistics and spatial correlation dimensions of earthquakes at Long Valley caldera, California, *Geophys. J. Int.*, *138*, 563–570, 1999.
- Benz, H. M., B. A. Chouet, P. B. Dawson, J. C. Lahr, R. A. Page, and J. A. Hole, Three-dimensional P and S wave velocity structure of Redoubt volcano, Alaska, *J. Geophys. Res.*, *101*, 8111–8128, 1996.
- Boitnott, G. N., Laboratory measurements on reservoir rocks from The Geysers geothermal field, paper presented at Twentieth Workshop on Geothermal Reservoir Engineering, Stanford Univ., Stanford, Calif., 1995.
- Boitnott, G. N., and P. J. Boyd, Permeability, electrical impedance, and acoustic velocities on reservoir rocks from The Geysers geothermal field, paper presented at Twenty-first Workshop on Geothermal Reservoir Engineering, Stanford Univ., Stanford, Calif., 1996.
- Borcherdt, R. D., J. B. Fletcher, E. G. Jensen, G. L. Maxwell, J. R. VanSchaack, R. E. Warrick, E. Cranswick, M. S. J. Johnston, and R. McClearn, A general earthquake-observation system (GEOS), *Bull. Seismol. Soc. Am.*, *75*, 1783–1825, 1985.
- Cramer, C. H., and S. R. McNutt, Spectral analysis of earthquakes in the 1989 Mammoth Mountain swarm near Long Valley, California, *Bull. Seismol. Soc. Am.*, *87*, 1454–1462, 1997.
- Denlinger, R. P., F. S. Riley, J. K. Boling, and M. C. Carpenter, Deformation of Long Valley caldera between August 1982 and August 1983, *J. Geophys. Res.*, *90*, 11,199–11,209, 1985.
- Eichelberger, J. C., P. C. Lysner, and L. W. Younker, Research drilling at Inyo Domes, Long Valley caldera, California, *Eos Trans. AGU*, *65*, 721, 723–725, 1984.
- Evans, J. R., D. Eberhart-Phillips, and C. H. Thurber, User's manual for SIMULPS12 for imaging V_p and V_p/V_s , a derivative of the Thurber tomographic inversion SIMUL3 for local earthquakes and explosions, *U.S. Geol. Surv. Open File Rep.*, *94-431*, 142 pp., 1994.
- Farrar, C. D., M. L. Sorey, W. C. Evans, J. F. Howle, B. D. Kerr, B. M. Kennedy, C.-Y. King, and J. R. Southon, Forest-killing diffuse CO₂ emission at Mammoth Mountain as a sign of magmatic unrest, *Nature*, *376*, 675–678, 1995.
- Fink, J. H., The geometry of silicic dikes beneath the Inyo domes, California, *J. Geophys. Res.*, *90*, 11,127–11,133, 1985.
- Foulger, G. R., and D. R. Toomey, Structure and evolution of the Hengill-Grensdalur volcanic complex, Iceland: Geology, geophysics, and seismic tomography, *J. Geophys. Res.*, *94*, 17,511–17,522, 1989.
- Foulger, G. R., A. D. Miller, B. R. Julian, and J. R. Evans, Three-dimensional V_p and V_p/V_s structure of the Hengill triple junction and geothermal area, Iceland, and the repeatability of tomographic inversion, *Geophys. Res. Lett.*, *22*, 1309–1312, 1995.
- Foulger, G. R., C. C. Grant, A. Ross, and B. R. Julian, Industrially induced changes in Earth structure at The Geysers geothermal area, California, *Geophys. Res. Lett.*, *24*, 135–137, 1997.

- Foulger, G. R., B. R. Julian, D. P. Hill, G. Sharer, L. E. Foulger, R. Perthro, N. Dotson, A. M. Pitt, and E. Brodsky, A Microearthquake Survey of the Mammoth Mountain area, Long Valley caldera, California, summer 1997, *U.S. Geol. Surv. Open File Rep.*, 98-236, 1998a.
- Foulger, G. R., P. E. Malin, E. Shalev, B. R. Julian, and D. P. Hill, Seismic monitoring and activity increase in California caldera, *Eos Trans. AGU*, 79, 357–363, 1998b.
- Gassmann, F., Über die elastizität poroser medien, *Verteljahrsschr. Naturforsch. Ges. Zurich*, 96, 1–23, 1951.
- Gerlach, T. M., M. P. Doukas, K. A. McGee, and R. Kessler, Airborne detection of diffuse carbon dioxide emissions at Mammoth Mountain, California, *Geophys. Res. Lett.*, 26, 3661–3664, 1999.
- Gunasekera, R. C., G. R. Foulger, and B. R. Julian, Four-dimensional tomography showing progressive pore fluid depletion at The Geysers geothermal area, California, *J. Geophys. Res.*, 108, 10.1029/2001JB000638, in press, 2003.
- Hill, D. P., Temperatures at the base of the seismogenic crust beneath Long Valley Caldera, California, and the Phlegrean Fields Caldera, Italy, in *Volcanic Seismology, IAVCEI Proceedings in Volcanology 3*, edited by P. Gasparini, R. Scarpa, and K. Aki, pp. 432–461, Springer-Verlag, New York, 1992.
- Hill, D. P., Earthquakes and carbon dioxide beneath Mammoth Mountain, California, *Seismol. Res. Lett.*, 67, 8–15, 1996.
- Hill, D. P., R. A. Bailey, and A. S. Ryall, Active tectonic and magmatic processes beneath Long Valley caldera, eastern California: An overview, *J. Geophys. Res.*, 90, 11,111–11,120, 1985a.
- Hill, D. P., J. H. Kissling, J. H. Luetgert, and U. Kradolfer, Constraints on the upper crustal structure of the Long Valley–Mono craters volcanic complex, eastern California, from seismic refraction measurements, *J. Geophys. Res.*, 90, 11,135–11,150, 1985b.
- Hill, D. P., W. L. Ellsworth, M. J. S. Johnston, J. O. Langbein, D. H. Oppenheimer, A. M. Pitt, P. A. Reasenberg, M. L. Sorey, and S. R. McNutt, The 1989 earthquake swarm beneath Mammoth Mountain, California: An initial look at the 4 May through 30 September activity, *Bull. Seismol. Soc. Am.*, 80, 325–339, 1990.
- Julian, B. R., An efficient program to locate earthquakes in one- and three-dimensional Earth models, U.S. Geol. Surv., Reston, Va., 2000.
- Julian, B. R., A. Ross, G. R. Foulger, and J. R. Evans, Three-dimensional seismic image of a geothermal reservoir: The Geysers, California, *Geophys. Res. Lett.*, 23, 685–688, 1996.
- Julian, B. R., A. M. Pitt, and G. R. Foulger, Seismic image of a CO₂ reservoir beneath a seismically active volcano, *Geophys. J. Int.*, 133, 7–10, 1998.
- Kissling, E., Geotomography with local earthquake data, *Rev. Geophys.*, 26, 659–698, 1988.
- Kissling, E., W. L. Ellsworth, D. Eberhart-Phillips, and U. Kradolfer, Initial reference models in local earthquake tomography, *J. Geophys. Res.*, 99, 19,635–19,646, 1994.
- Krief, M., J. Garat, J. Stellingwerff, and J. Ventre, A petrophysical interpretation using the velocities of P and S waves, *Log Anal.*, 31, 355–369, 1990.
- Langbein, J., Deformation of the Long Valley caldera, eastern California, from mid-1983 to mid-1988; measurements using a two-color geodimeter, *J. Geophys. Res.*, 94, 3833–3850, 1989.
- Langbein, J., D. P. Hill, T. N. Parker, and S. K. Wilkinson, An episode of reinflation of the Long Valley caldera, eastern California: 1989–1991, *J. Geophys. Res.*, 98, 15,851–15,870, 1993.
- Langbein, J. D., D. Dzurizin, G. Marshall, R. Stein, and J. Rundle, Shallow and peripheral volcanic sources of inflation revealed by modeling two-color geodimeter and leveling data from Long Valley caldera, California, *J. Geophys. Res.*, 100, 12,487–12,495, 1995.
- Mavko, G., and T. Mukerji, Seismic pore space compressibility and Gassmann's relation, *Geophysics*, 60, 1743–1749, 1995.
- Mavko, G., C. Chan, and T. Mukerji, Fluid substitution: Estimating changes in V_p without knowing V_s , *Geophysics*, 60, 1750–1755, 1995.
- McConnell, J. S., C. K. Shearer, J. C. Eichelberger, M. J. Keskinson, P. W. Layer, and J. J. Papike, Rhyolite intrusions in the intracaldera Bishop Tuff, Long Valley caldera, California, *J. Volcanol. Geotherm. Res.*, 67, 41–60, 1995.
- McGee, K. A., T. M. Gerlach, R. Kessler, and M. P. Doukas, Geochemical evidence for a magmatic CO₂ degassing event at Mammoth Mountain, California, September–December 1997, *J. Geophys. Res.*, 105, 8447–8456, 2000.
- Miller, A. D., B. R. Julian, and G. R. Foulger, Three-dimensional seismic structure and moment tensors of non-double-couple earthquakes at the Hengill-Grensdalur volcanic complex, Iceland, *Geophys. J. Int.*, 133, 309–325, 1998.
- Miller, C. D., Holocene eruptions at the Inyo Craters volcanic chain, California: Implications for possible eruptions in Long Valley caldera, *Geology*, 13, 14–17, 1985.
- Pitt, A. M., and D. P. Hill, Long-period earthquakes in the Long Valley caldera region, eastern California, *Geophys. Res. Lett.*, 21, 1679–1682, 1994.
- Rundle, J. B., and D. P. Hill, The geophysics of a restless caldera—Long Valley, California, *Annu. Rev. Earth Planet. Sci.*, 16, 251–271, 1988.
- Sanders, C. O., Location and configuration of magma bodies beneath Long Valley, California, determined from anomalous earthquake signals, *J. Geophys. Res.*, 89, 8287–8302, 1984.
- Sanders, C. O., and F. Ryall, Geometry of magma bodies beneath Long Valley, California, determined from anomalous earthquake signals, *Geophys. Res. Lett.*, 10, 690–692, 1983.
- Sorey, M. L., Evolution and present state of the hydrothermal system in Long Valley caldera, *J. Geophys. Res.*, 90, 11,219–11,228, 1985.
- Sorey, M. L., B. M. Kennedy, C. D. Farrar, and G. A. Suemnicht, Helium isotope and gas discharge variations associated with crustal unrest in Long Valley caldera, California, 1989–1992, *J. Geophys. Res.*, 98, 15,871–15,889, 1993.
- Sorey, M. L., W. C. Evans, B. M. Kennedy, C. D. Farrar, L. J. Hainsworth, and B. Hausback, Carbon dioxide and helium emissions from a reservoir of magmatic gas beneath Mammoth Mountain, California, *J. Geophys. Res.*, 103, 15,303–15,323, 1998.
- Stroujkova, B. F., and P. E. Malin, A magma mass beneath Casa Diablo? Further evidence from reflected seismic waves, *Bull. Seismol. Soc. Am.*, 90, 500–522, 2000.
- Thurber, C. H., Earthquake locations and three-dimensional crustal structure in the Coyote Lake area, central California, *J. Geophys. Res.*, 88, 8226–8236, 1983.
- Tryggvason, A., Seismic tomography: Inversion for P- and S-wave velocities, Ph.D. thesis, Univ. of Uppsala, Uppsala, Sweden, 1998.
- Wang, Z., and A. M. Nur, Effects of CO₂ flooding on wave velocities in rocks with hydrocarbons, *Soc. Pet. Eng. Res. Eng.*, 3, 429–436, 1989.
- Wang, Z., M. E. Cates, and R. T. Langen, Seismic monitoring of CO₂ flooding of a carbonate reservoir: A rock physics study, *Geophysics*, 63, 1604–1617, 1998.
- Wessel, P., and W. H. F. Smith, New, improved version of Generic Mapping Tools released, *Eos Trans. AGU*, 79, 579, 1998.
- Wiemer, S., S. R. McNutt, and M. Wyss, Temporal and three-dimensional spatial analyses of the frequency-magnitude distribution near Long Valley caldera, California, *Geophys. J. Int.*, 134, 409–421, 1998.

G. R. Foulger, Department of Geological Sciences, University of Durham, Science Laboratories, South Rd., Durham DH1 3LE, UK. (g.r.foulger@durham.ac.uk)

D. P. Hill, B. R. Julian, and A. M. Pitt, Volcano Hazards Team, U.S. Geological Survey, 345 Middlefield Rd., MS 977, Menlo Park, CA 94025, USA.

P. E. Malin and E. Shalev, Division of Earth and Ocean Sciences, Nicholas School of the Environment, Duke University, Box 90235, Durham, NC 27708-0235, USA.